arXiv:1402.3853v1 [physics.chem-ph] 16 Feb 2014

Photoelectron angular distributions from aligned molecules using the R-matrix method

Alex G Harvey, Danilo S Brambila, Felipe Morales and Olga Smirnova

Max-Born-Institut, Max-Born-Strasse 2A, D-12489 Berlin, Germany

E-mail: harvey@mbi-berlin.de

Abstract. We present a new extension of the UKRmol electron-molecule scattering code suite, which allows one to compute *ab initio* photoionization and photorecombination amplitudes for complex molecules, resolved both on the molecular alignment (orientation) and the emission angle and energy of the photoelectron. We illustrate our approach using CO_2 as an example, and analyze the importance of multi-channel effects by performing our calculations at different, increasing levels of complexity. We benchmark our method by comparing the results of our calculations with experimental data and with theoretical calculations available in the literature.

PACS numbers: 33.60.+q, 33.80.Eh, 82.53.Kp

1. Introduction

The goal of attosecond spectroscopy is to observe non-equilibrium multi-electron dynamics on its natural, attosecond, time-scale. In the family of recently developed approaches, including high harmonic generation (HHG) spectroscopy [1, 2, 3], the attosecond streak camera [4], the reconstruction of attosecond bursts by interference of two-photon transitions (RABBITT) method [5, 6], laser-induced electron diffraction [7, 8, 9], attosecond resolution comes hand in hand with the application of intense IR or XUV pulses and usually involves ionization of the target. The attosecond dynamics are often mapped onto, and have to be read out from, the atomic or molecular continuum. These attosecond dynamics can be decoded from experimental observables using semi-classical methods [10, 11, 12], which often allow one to break the full process into separate, coherent steps, e.g. ionization, continuum dynamics, recombination or scattering. Decoding such attosecond dynamics requires the development of theoretical methods capable of describing angle and energy resolved photoionization/photorecombination dipoles and scattering amplitudes. Accurate treatment of the molecular continuum is crucial for pushing attosecond spectroscopy to complex molecules. Most attosecond experiments are done with aligned molecules, but angular and energy resolved dipoles are often required even in the case of unaligned or weakly aligned targets to account for the coherence between different pathways associated with different alignment angles. For example, coherent addition of light emitted during the recombination of an electron with its parent molecular ion, for different molecular orientations, is crucial for HHG spectroscopy. Significant advances in HHG spectroscopy are associated with the application of the Schwinger variational method for calculating photoionization/photorecombination dipoles [13]. Here we present a new development based on the extension of the UKRmol [14] electron-molecule scattering codes, which allows one to compute dipole matrix elements, and photoionization and recombination cross-sections, resolved in alignment, emission angle and energy, for complex molecules. As an example, we consider the application of the new codes to the CO_2 molecule.

We note that there have been relatively few applications of the R-matrix approach to molecular photoionization [15, 16, 17, 18] and they have primarily looked at orientationally averaged observables, the exception being the single channel, finite element, R-matrix code, FERM3D [19].

2. Theory

2.1. Overview

Initially proposed by Wigner and Eisenbud [20] in the 1940s for the characterization of resonant nuclear scattering, the R-matrix method has undergone, over the years, significant adaptation and development to treat electron-atom and electron-molecule interactions. We will present here just those elements of R-matrix theory required to describe our new development. For comprehensive discussion of R-matrix techniques and applications, as applied to electron and photon induced processes in atomic and molecular physics, the recent review [21], and book [22] are excellent starting points.

The R-matrix technique is a method of solving the, inherently multi-channel, electron-(photon)-molecule collision problem within the close coupling approximation. The power of the R-matrix approach lies in the division of the configuration space of

the molecule into separate regions; this division allows one to apply the appropriate approximation and optimal computational technique in each region.

The usual division is into an inner region, close to the molecule, where the non-local electron-electron exchange and correlation interactions are important, and must be accounted for; an outer region, where the continuum electron is distinguishable from the bound electrons, non-local exchange and correlation are negligible, and the problem reduces to the ejected electron scattering in the long-range multi-pole potential of the parent molecule; and an asymptotic region, where the long-range potential is weak, and the solution is well represented by an asymptotic expansion which satisfies the physical boundary conditions.

In the inner region the continuum is discretized, allowing the use of basis set methods adapted from quantum chemistry. In the outer region numerical integration techniques are used to propagate the inner region solutions from the boundary to the asymptotic region, where matching to the asymptotic expansion applies the appropriate physical boundary conditions.

2.2. Dipoles and cross sections

UKRmol calculations are performed in the molecular frame, so in the following discussion we start from the molecular frame description of photoionization and, towards the end, transform to the laboratory frame. Along the way we will indicate the new (in contrast to a scattering calculation) quantities that we require.

In the theoretical description of single photon ionization [23], within the length gauge dipole approximation, the molecular frame photo-electron angular distribution can be expressed as,

$$\frac{\mathrm{d}\sigma_{fi}}{\mathrm{d}\boldsymbol{k}_f} = 4\pi^2\alpha a_0^2\omega|\boldsymbol{d}_{fi}(\boldsymbol{k}_f)\cdot\hat{\boldsymbol{\epsilon}}|^2, \tag{1}$$

where α is the fine structure constant, a_0 is the Bohr radius, ω is the photon energy in atomic units, and $\hat{\boldsymbol{\epsilon}}$ is the polarization direction of the incident photon in the molecular frame. The molecular frame transition dipole, $\boldsymbol{d}_{fi}(\boldsymbol{k}_f)$, between an initial bound state, Φ_i^N, and a final continuum state, $\Psi^{(-)}_{f\boldsymbol{k}_f}$, of the molecule is,

$$\boldsymbol{d}_{fi}(\boldsymbol{k}_f) = \langle\Psi^{(-)}_{f\boldsymbol{k}_f}|\boldsymbol{d}|\Phi_i^N\rangle, \tag{2}$$

where $\boldsymbol{d}$ is the dipole operator, the momentum of the ejected electron is $\boldsymbol{k}_f$, and the ion is left in the state indexed by f. We use the length gauge form of the dipole operator, which can be written in spherical vector form as,

$$d_q = \left(\frac{4\pi}{3}\right)^{1/2}\sum_{i=1}^{N} r_i Y_{1,q}(\hat{\boldsymbol{r}}_i), \tag{3}$$

where $\hat{\boldsymbol{r}}_i$ is the coordinate of the i-th electron and $Y_{1,q}(\hat{\boldsymbol{r}}_i)$ is a spherical harmonic. The $q=\pm1$ components correspond to circular polarization and the $q=0$ component to linear polarization.

If we only consider initial states that fit in the inner region, the integral above can be restricted to the inner region and we can expand both the initial and final state

in terms of the energy independent inner region solutions $\psi_k^{(N)}$.

$$\Psi_{f\boldsymbol{k}_f}^{(-)} = \sum_k A_{fk}(\boldsymbol{k}_f)\psi_k^{(N)} \tag{4}$$

$$\Phi_i^N \quad = \sum_k B_{ik}\psi_k^{(N)} \tag{5}$$

The transition dipole becomes

$$\boldsymbol{d}_{fi}(\boldsymbol{k}_f) = \sum_{kk'} A_{fk}^*(\boldsymbol{k}_f)\langle\psi_k^{(N)}|\boldsymbol{d}|\psi_{k'}^{(N)}\rangle B_{ik'}, \tag{6}$$

The R-matrix codes work in the angular momentum basis for the ejected electron, in a partial wave expansion, as the expansion often converges for low values of l. In this basis, eq. 6 becomes,

$$\begin{aligned}\boldsymbol{d}_{fi}(\boldsymbol{k}_f) = \sum_{kk'}\sum_{l_f m_f} & i^{-l_f}e^{i\sigma_{l_f}}Y_{l_f,m_f}(\hat{\boldsymbol{k}}_f)(S_f M_{S_f}\tfrac{1}{2}m_{s_f}|SM_S) \\ & A_{fl_f m_f,k}^*(E)\langle\psi_k^{(N)}|\boldsymbol{d}|\psi_{k'}^{(N)}\rangle B_{ik'},\end{aligned} \tag{7}$$

here $\sigma_{l_f} = \arg\Gamma(l_f+1+i\eta_f)$ is the Coulomb phase, with $\eta_f = -\frac{Z-(N-1)}{k_f}$, where $Z-(N-1)$ is the residual charge on the the ion. The Clebsch-Gordan coefficient is due to spin coupling of the continuum electron and the ion. The partial wave dipole is defined as follows.

$$\boldsymbol{d}_{fl_f m_f,i}(E) = \sum_{kk'} A_{fl_f m_f,k}^*(E)\langle\psi_k^{(N)}|\boldsymbol{d}|\psi_{k'}^{(N)}\rangle B_{ik'} \tag{8}$$

Clearly, to calculate transition dipoles and photoionization/recombination observables we need the expansion coefficients for the initial and final states in the inner region and transition dipoles between the inner region states. In contrast, only the expansion coefficients in terms of the asymptotic solutions are required to obtain scattering observables.

To connect to the lab frame observables, we introduce Euler angles α, β, γ, which define the rotation of molecule from the lab frame, and the associated Wigner rotation matrices (see, for example [24]), $\boldsymbol{D}^l(\alpha,\beta,\gamma)$. In the lab frame eq. 8 becomes,

$$\begin{aligned}\boldsymbol{d}'_{fi}(\boldsymbol{k}'_f) = \sum_{l_f m'_f m_f} & i^{-l_f}e^{i\sigma_{l_f}}Y_{l_f,m'_f}(\hat{\boldsymbol{k}}'_f)(S_f M_{S_f}\tfrac{1}{2}m_{s_f}|SM_S) \\ & D^l_{m'_f m_f}\boldsymbol{d}_{fl_f m_f,i}(E)\boldsymbol{D}^{1\dagger},\end{aligned} \tag{9}$$

where the primed variables indicate lab frame quantities. If the target molecule spins are unpolarized and the final state spins are not measured, one must average over the initial and sum over the final spin components.

$$\frac{\mathrm{d}\sigma_{fi}}{\mathrm{d}\boldsymbol{k}_f} = \frac{4\pi^2\alpha a_0^2\omega}{2S+1}\sum_{M_S,M_{S_f},m_{s_f}}|\boldsymbol{d}_{fi}(\boldsymbol{k}_f)\cdot\boldsymbol{\epsilon}|^2, \tag{10}$$

Finally, in addition to angular distributions from aligned molecules, we will present orientationally averaged partial photoionization cross sections for comparison to existing theory and experiment. With the aid of angular momentum algebra (see,

for example, [25]) the orientationally averaged partial photoionization cross section takes the following convenient form,

$$\sigma_{fi}(E) = \frac{4}{3}\pi^2 \alpha a_0^2 \omega \sum_{q l_f m_f} |d_{q,f l_f m_f,i}(E)|^2. \tag{11}$$

photoionization and recombination observables are produced by the new code module, DIPELM, which takes the expansion coefficients and inner region dipoles as input. In the next section, we describe the R-matrix approach to calculating the scattering wavefunction, $\Psi^{(-)}_{f\boldsymbol{k}_f}$.

2.3. Scattering states

The R-matrix method, as implemented by the UKRmol code suite, is a close-coupling approach to solving the scattering problem (within the fixed nuclei approximation), where the scattering wavefunction is expanded in terms of target states, with expansion coefficients dependent on the coordinate of the continuum electron.

2.3.1. Inner region In the inner region, the (discretized) continuum is represented by a set of continuum orbitals, η_{m_f}, and the close-coupling expansion takes the form

$$\begin{aligned}\psi_k^{(N)} = \mathcal{A} \sum_{f m_f} a_{k f m_f} \Phi_f^{(N-1)}(x_1, ..., x_{N-1}) \eta_{m_f}(x_N) \\ + \sum_p b_{kp} \chi_p^{(N)}(x_1, ..., x_{N-1}, x_N).\end{aligned} \tag{12}$$

The continuum orbitals are built from a set of Gaussian type orbitals (GTO) fitted to Coulomb or Bessel functions [26]. Molecular orbitals are constructed from a second set of GTO and used to create the target states, $\Phi_f^{(N-1)}$, using configuration interaction. $\chi_p^{(N)}$ are configurations created by placing the continuum orbital into a bound orbital and are needed to describe short-range correlation lost due to orthogonalization of bound and continuum orbitals. Exchange is treated rigorously by anti-symmetrization (the operator $\mathcal{A}$). The coefficients, $a_{k f m_f}$ and b_{kp}, are found by diagonalising the full electronic Hamiltonian restricted to the inner region [27]. The end result of this procedure is a flexible basis, $\psi_k^{(N)}$, with which to represent the N-electron wavefunction, for both bound and continuum states, in the inner region.

To connect to the outer region, the radial part of the inner region wavefunctions, evaluated on the R-matrix boundary is needed (only the continuum orbitals are non-zero on the boundary). These are known as the boundary amplitudes, w_{ik}, and are constructed by projection on to the channel functions as follows,

$$w_{ik}(a) = \langle \Phi_i^{(N-1)} Y_{l_i,m_i} | \psi_k^{(N)} \rangle. \tag{13}$$

The spherical harmonics, Y_{l_i,m_i}, are defined in the molecular frame and we note that the continuum is spin coupled to the target. The partial wave expansion of the continuum implicit in the above leads to each target state being associated with a number of degenerate partial wave channels. We denote the total number of these channels as n, with n_o energetically open and n_c closed. The single index, i, on the boundary amplitudes now indexes these channels. The $n \times n$ R-matrix is then constructed,

$$\mathbf{R}(a) = \frac{1}{2} \mathbf{w}(a) \left[\mathbf{E_k} - E\right]^{-1} \mathbf{w}^T(a), \tag{14}$$

where $[\mathbf{E_k} - E]^{-1}$ is a diagonal matrix with elements $\delta_{kk'}(E_k - E)^{-1}$. E_k are the eigenenergies of the $\psi_k^{(N)}$ and are known as the R-matrix poles. If Ψ_j is a solution of the full Hamiltonian, then projecting out the channel functions, and evaluating at $r = a$ as before gives us,

$$F_{ij}(a) = \langle \Phi_i^{(N-1)} Y_{l_i,m_i} | \Psi_j \rangle, \tag{15}$$

the R-matrix (in its simplest form) then relates $\mathbf{F}$ to its derivative,

$$\mathbf{F}(a) = \mathbf{R}(a)\mathbf{F}'(a). \tag{16}$$

2.3.2. Outer and asymptotic region The close coupling expansion in the outer region takes a simpler form,

$$\Psi_j = \sum_i \Phi_i^{(N-1)}(x_1, ..., x_{N-1}; \sigma_{N+1}) Y_{l_i,m_i}(\hat{r}_{N+1}) r_{N+1}^{-1} F_{ij}(r_{N+1}) \tag{17}$$

where the summation over i is a summation over the partial wave channels. Substituting into the Schrdinger equation and projecting out the channel functions give the reduced radial equations,

$$\left[\frac{\mathrm{d}^2}{\mathrm{d}r^2} - \frac{l_i(l_i+1)}{r^2} + \frac{2(Z-(N-1))}{r} + k_i^2\right] F_{ij} = 2\sum_{i'=1}^{n} V_{ii'} F_{i'j}. \tag{18}$$

Of the $2n$ linearly independent solutions to the reduced radial equations, n are divergent at the origin and n_c are divergent asymptotically, and thus, are physically inadmissible. This leaves n_o independent solutions. $\boldsymbol{F}$ has standing wave asymptotic boundary conditions,

$$\boldsymbol{F} \sim \mathbf{k}^{-1/2}[\mathbf{S} + \mathbf{CK}], \tag{19}$$

where $\mathbf{S}$ is the matrix of fundamental solutions with sine like asymptotic behaviour $\mathbf{C}$ is cosine like for open channels and exponentially decaying for closed channels. Computationally, it is useful to apply standing wave boundary conditions and solve for the K-matrix as it avoids the need for complex numbers in the calculation until the end. Conversion to incoming, $\boldsymbol{F}^-$, or outgoing wave, $\boldsymbol{F}^+$, boundary conditions appropriate for photoionization and recombination respectively is straightforward.

$$\boldsymbol{F}^{\pm} = \sqrt{\frac{2}{\pi}}\boldsymbol{F}[\mathbf{1} \mp i\mathbf{K}]^{-1}. \tag{20}$$

2.3.3. Expansion coefficients Eq. (5) allows us to write the radial wavefunction in terms of the expansion coefficients and boundary amplitudes as follows,

$$\boldsymbol{F}^{\pm} = \mathbf{w}\boldsymbol{A}^{\pm}, \tag{21}$$

remembering that the R-matrix relates the radial function and its derivative we can write

$$\mathbf{w}\boldsymbol{A}^{\pm} = \mathbf{R}\boldsymbol{F}'^{\pm} \tag{22}$$

$$= \frac{1}{2}\mathbf{w}\left[\mathbf{E_k} - E\right]^{-1}\mathbf{w}^T\boldsymbol{F}'^{\pm} \tag{23}$$

from which it is easy to see that

$$\mathbf{A}^{\pm} = \frac{1}{2}\left[\mathbf{E_k} - E\right]^{-1}\mathbf{w}^T\mathbf{F}'^{\pm} \tag{24}$$

or alternatively

$$\mathbf{A}^{\pm} = \frac{1}{2}\left[\mathbf{E_k} - E\right]^{-1}\mathbf{w}^T\mathbf{R}^{-1}\mathbf{F}^{\pm}. \tag{25}$$

To obtain the expansion coefficient all quantities need to be evaluated at a single radius. However, following a standard scattering calculation we have the boundary amplitudes defined only at the R-matrix boundary, a, and the radial function defined only at the matching radius, c. R-matrix propagation is performed using the technique of Baluja *et al.* [28] where a set of four matrices, $\{\mathcal{R}_{11}, \mathcal{R}_{12}, \mathcal{R}_{21}, \mathcal{R}_{22}\}$, are constructed which relate the R-matrix at a to the R-matrix at c as follows,

$$\mathbf{R}(c) = \mathcal{R}_{22} - \mathcal{R}_{21}[\mathcal{R}_{11} + \mathbf{R}(a)]^{-1}\mathcal{R}_{12} \tag{26}$$

$$\mathbf{R}(a) = \mathcal{R}_{12}[\mathcal{R}_{22} - \mathbf{R}(c)]^{-1}\mathcal{R}_{21} - \mathcal{R}_{11}. \tag{27}$$

We also have the relation,

$$\mathbf{F}(a) = \mathcal{R}_{12}\mathbf{F}'(c) - \mathcal{R}_{11}\mathbf{F}'(a) \tag{28}$$

$$\mathbf{F}(c) = \mathcal{R}_{22}\mathbf{F}'(c) - \mathcal{R}_{21}\mathbf{F}'(a), \tag{29}$$

which can be rearranged to give,

$$\mathbf{F}(a) = \mathcal{R}_{12} - \mathcal{R}_{11}\mathcal{R}_{21}^{-1}[\mathcal{R}_{22} - \mathbf{R}(c)]\mathbf{F}'(c) \tag{30}$$

$$\mathbf{F}'(a) = \mathcal{R}_{21}^{-1}[\mathcal{R}_{22}\mathbf{F}'(c) - \mathbf{F}(c)]. \tag{31}$$

This gives us the radial functions back propagated to the R-matrix boundary allowing construction of the wavefunction coefficients. We note that some care must be taken near channel thresholds where numerical instability can occur. Generally this can be avoided by increasing the forward propagation distance and, if necessary, increasing the numerical precision under which the linear algebra is performed. Expansion coefficients are calculated by a new outer region routine, COMPAK.

2.4. Bound states and inner region dipoles

Bound states required to describe the initial(/final) state for photoionization(/recombination) can be produced in several ways: they can be constructed using standard quantum chemistry techniques, with the proviso that the same set of orbitals must be used as was used for the target calculation; they can be constructed from the inner region wavefunctions by considering all channels to be closed, using the outer region module BOUND [29]; lastly, it can be a good approximation to take the lowest energy inner region wavefunction of the appropriate symmetry to represent the ground state of the neutral molecule [18].

Transition dipoles between inner region wavefunctions are calculated using a new, optimized and extended, version of DENPROP that can directly use the close coupling basis of eq. (12), CDENPROP (detailed elsewhere, [30]).

3. CO_2: Models

3.1. Target

The first step in a R-matrix calculation is construction of the target states, in the case of CO_2 photoionization, states of CO_2^+ at the equilibrium bond length of the neutral (for previous work on scattering from CO_2^+ using UKRmol see [31, 32, 33]). A set of molecular orbitals were constructed from an initial Gaussian basis set (cc-pVTZ)

Table 1: Target models: The bracket exponents denote the number of electrons placed in the set of orbitals contained in the bracket. The configurations column lists the maximum number of configurations used to represent a target state in that model (there is a small symmetry dependence to the number of configurations).

Model	Active space	CSFs
Model 1	$(1\text{-}2\sigma_g, 1\sigma_u)^6(3\text{-}4\sigma_g, 2\text{-}3\sigma_u, 1\pi_u 1\pi_g)^{15}$	1
Model 2	$(1\text{-}2\sigma_g, 1\sigma_u)^6(3\text{-}4\sigma_g, 2\text{-}3\sigma_u, 1\pi_u 1\pi_g)^{15}$	440
	$(1\text{-}2\sigma_g, 1\sigma_u)^6(3\text{-}4\sigma_g, 2\text{-}3\sigma_u, 1\pi_u 1\pi_g)^{14}(5\sigma_g, 2\pi_u, 4\sigma_u)^1$	
	$(1\text{-}2\sigma_g, 1\sigma_u)^6(3\text{-}4\sigma_g, 2\text{-}3\sigma_u, 1\pi_u 1\pi_g)^{13}(5\sigma_g, 2\pi_u, 4\sigma_u)^2$	
Model 3	$(1\text{-}2\sigma_g, 1\sigma_u)^6(3\text{-}5\sigma_g, 2\text{-}3\sigma_u, 1\text{-}2\pi_u 1\pi_g)^{15}$	3692

Table 2: Target energies (eV) relative to the groundstate for the various models, in comparison to experiment [38]. Bracketed figures: difference with experiment.

State	Model 1	Model 2	Model 3	Experiment
$X^2\Pi_g$	0.00	0.00	0.00	0.0
$A^2\Pi_u$	4.70 (0.90)	4.12 (0.32)	3.97 (0.17)	3.8
$B^2\Sigma_u^+$	5.33 (1.03)	4.77 (0.47)	4.45 (0.15)	4.3
$C^2\Sigma_g^+$	7.14 (1.54)	5.97 (0.37)	5.77 (0.17)	5.6

[34] using a state averaged CASSCF [35, 36] procedure with the quantum chemistry package Molpro [37]. 21 states of the ion and the ground state of the neutral were included in the averaging. Choice of orbital set can have a strong influence on shape resonance features; in the spirit of the frozen core Hartree-Fock approximation, we chose the state averaging to be predominantly weighted towards the neutral with a small (10%) component of ionic states to improve the description of the target.

We note here that UKRmol is restricted to the use of abelian point groups, therefore D_{2h} is the highest symmetry that can be used for CO_2. Where target states are degenerate we include both states (corresponding to two different irreducible representations in D_{2h}), this also has consequences for the treatment of the continuum, as a basis of real (tesseral) spherical harmonics, the appropriate angular basis for D_{2h} and its subgroups, is used instead of the usual complex spherical harmonics. This leads to some necessary modifications of eq. (7-9), which are detailed in the appendix. We looked at three different target models of increasing complexity (see table 1). All models have 6 electrons frozen in the core orbitals $(1-2\sigma_g, 1\sigma_u)$. Model 1 represents the target states with a single configuration state function (CSF) and thus does not include electronic correlation in the ion. Model 2 includes single and double excitations into the valence orbitals not included in model 1. Model 3 consists of the full valence complete active space minus the $4\sigma_u$ orbital. Table 2 shows the energies of the lowest 4 ionic states. Model 1 gives generally poor agreement with experimental energies, model 2, is significantly better, and model 3 agrees to within 0.2 eV.

The lowest inner region wavefunction of the appropriate symmetry was used as the ground state of the neutral.

3.2. Inner region

Continuum orbitals up to $l = 5$ and spanning an energy range from 0 to 3.5 Hartree were generated by optimizing a set of GTO to represent Coulomb functions. 3 virtual orbitals were included in each symmetry to improve the description of inner region polarization. Single channel calculations were performed using the model 1 description of the ion and multichannel calculations with models 2 and 3. With model 2 and 3 we included 96 states in the close coupling expansion.

3.3. Outer region

We matched to Coulomb functions at the R-matrix boundary: for molecules, such as CO_2, with no permanent dipole, this approximation works well, at least at the level of the background cross section and shape resonances, and offers significant computational saving when there are many channels. Narrow resonance features however, are sensitive to channel coupling in the outer region and we would not expect to get good positions and widths without outer region propagation.

4. CO_2: Results

4.1. Partial cross sections

Fig. (1) shows orientationally averaged partial cross sections leaving the ion in the ground and first three excited states. The first feature to note is the presence of a high number of narrow resonance features in the R-matrix cross sections, these are autoionizing resonances associated with the various excitation thresholds included in the models. The single channel cross sections, with no excitation, are smooth. The experimental results we compare to here are of insufficient resolution to resolve the resonances, and the accurate characterization of such resonances, traditionally a strength of R-matrix approaches, has been left for future work. In this work we concern ourselves with the background cross sections and broader shape resonance features.

The agreement with experiment and previous theory is excellent, with the CI models (2 and 3) generally in better agreement, up to 45 eV, than model 1. Above 45 eV the CI models display some unphysical pseudoresonances related to the omission of highly excited states in the close coupling expansion that are implicitly included in the second summation of eq. (12). Model 1, the single channel, static exchange model, gives slightly worse resonance positions compared to the previous work [39] (labelled Lucchese: 1 chan in the figures) at a similar level of approximation performed using the Schwinger variational approach. This difference is primarily due to the choice of orbitals (neutral HF vs state averaged CASSCF over both neutral and ionic states); our orbital choice includes some degree of orbital relaxation which tends to shift resonance positions to higher energy. Another difference is in the choice of gauge, our work uses the length gauge, as opposed to a mixed gauge approach in the previous theoretical work.

Previous theoretical work found a high, narrow shape resonance in the C channel at around 42 eV, approximately 5 eV above the IP of the ion, that was not evident in experimental cross sections. Various attempts to reconcile theory and experiment were made at the time, including vibrational averaging [40], and the inclusion of channel coupling and initial state correlation [41, 39], with partial success. It was speculated

that the discrepancy was due to the need for correlation in the ion and many more excited states of the ion to be included in the channel coupling. Model 2 and 3 include both these and give very good agreement to experiment. In Fig (2) we see that the number of ionic channels plays a strong role in suppression of the resonance. With 64 states included the resonance is somewhat lowered in amplitude and significantly shifted in position, going to 96 states only has a small effect on position, but a dramatic effect on resonance height, which we attribute to loss of flux into highly excited ionic states.

Finally we note that cross sections near to and beyond the IP of the ion must be treated with some caution; for reliable treatment of the intermediate energy range (from close to the ionization threshold of the target up to several times this threshold), it has been found to be important in the accurate calculation of scattering and photoionization observables to account for highly excited electronic states of the target and the target continuum that are not included in the standard close-coupling approach. An approach that has found a great deal of success in atomic photoionization and scattering calculations and is beginning to be applied to the molecular case is the R-matrix with pseudostates method (RMPS) [42]. As well as a rigorous treatment of the intermediate energy regime, RMPS has the benefit of converging the polarizability of the ion, which can have a strong effect on resonance position.

4.2. Photoelectron angular distributions

Two common experimental alignment distributions are: aligned with with the photon polarization and planar delocalized perpendicular (anti-aligned) to the photon polarization. These arise in the impulsive laser alignment of molecules, where a rotational wavepacket is produced that cycles between alignment, anti-alignment and random alignment [48, 49, 50, 51, 52]. In this section we present photo-electron angular distributions (PAD) for these two scenarios.

Figures 3 and 4 show the $p_z - p_x$ emission plane for aligned and anti-aligned molecules respectively. The lab $z-$axis is defined by the (linearly polarized) photon polarization. In both these cases the cylindrical symmetry of the system is preserved leading to a cylindrically symmetric (around the $z-$axis) PAD. We therefore lose no information in looking at a 2D momentum cut.

We see that both aligned and anti-aligned results have rich angular structure, one useful method for the interpretation of angular distributions is to consider the angular momentum of the ejected photo-electron, the angular pattern in a particular energy region can be dominated by a particular partial wave, such as when there is a resonance in that partial wave, and interference between partial waves is a sensitive probe of the photoelectron-ion potential [53].

The ground state of the neutral has $^1\Sigma_g$ symmetry, for the aligned case the dipole operator has σ_u symmetry leading to final state symmetry of $^1\Sigma_u$. This leads to a π_u, π_g, σ_g and σ_u symmetry of the continuum in the X, A, B and C channels respectively. For the anti-aligned case the dipole operator has π_u symmetry leading to final state symmetry of $^1\Pi_u$. This leads to a σ_u, σ_g, π_g and π_u, symmetry of the continuum in the X, A, B and C channels respectively. σ and π continua correspond to partial waves with $|m| = 0$ and $|m| = 1$ respectively. l is even or odd (gerade or ungerade) and a particular partial wave has $|m|$ longitudinal nodes $l - |m|$ latitudinal nodes. Taking the X channel in the aligned case as an example we can see that it is dominated by

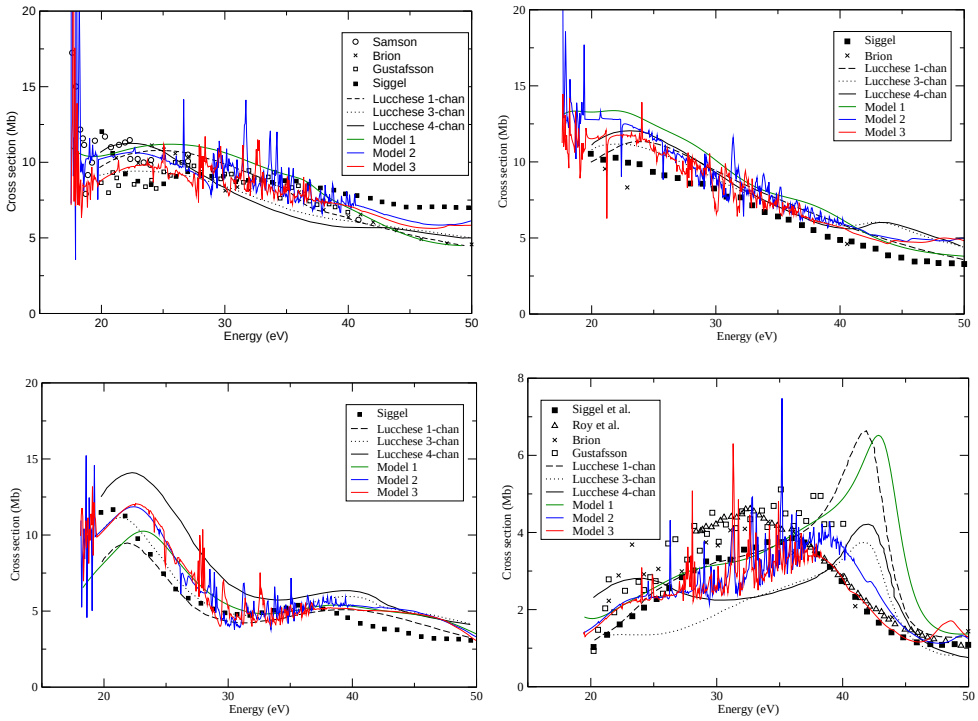

Figure 1: Partial cross sections: Top left, final ion state $X^2\Pi_g$. Top right, $A^2\Pi_u$. Bottom left, $B^2\Sigma_u^+$. Bottom right, $C^2\Sigma_g^+$. Experimental results: Samson et al. [43], Gustaffsson et al. [44], Siggel et al. [45], Brion and Tan [46] and Roy et al. [47]. Previous thoeretical results, Lucchese et al. [39]

the $l = 3$ partial wave, with a smaller contribution from $l = 1$, between 20 and 30 eV. At higher energies, from 40 eV the $l = 5$ partial wave becomes dominant.

5. Conclusions

We have presented extensions to the polyatomic UKRmol electron-molecule scattering codes that allow calculation of photoionization and recombination, from both oriented and orientationally averaged molecules. Our new codes have been applied to CO_2, with good agreement to experiment and alternative theoretical techniques for orientationally averaged quantities. The inclusion of both correlation, and channel coupling between many highly excited states of the ion was found to be important for the accurate description of the shape resonance in the $C^2\Sigma_g^+$ partial photoionization cross section. We note that our angularly resolved calculations have been used in two joint theoretical-experimental studies of aligned CO_2, the first measures photoelectron angular distributions from aligned CO_2 using a HHG photon source [54], the second measured HHG from aligned CO_2 (Harvey et al. in prep.). In both cases good agreement between theory and experiment was achieved. We anticipate that, as has been the case for atoms, the R-matrix approach to photoionization will be a fruitful method for the accurate study of photoionization and recombination processes in

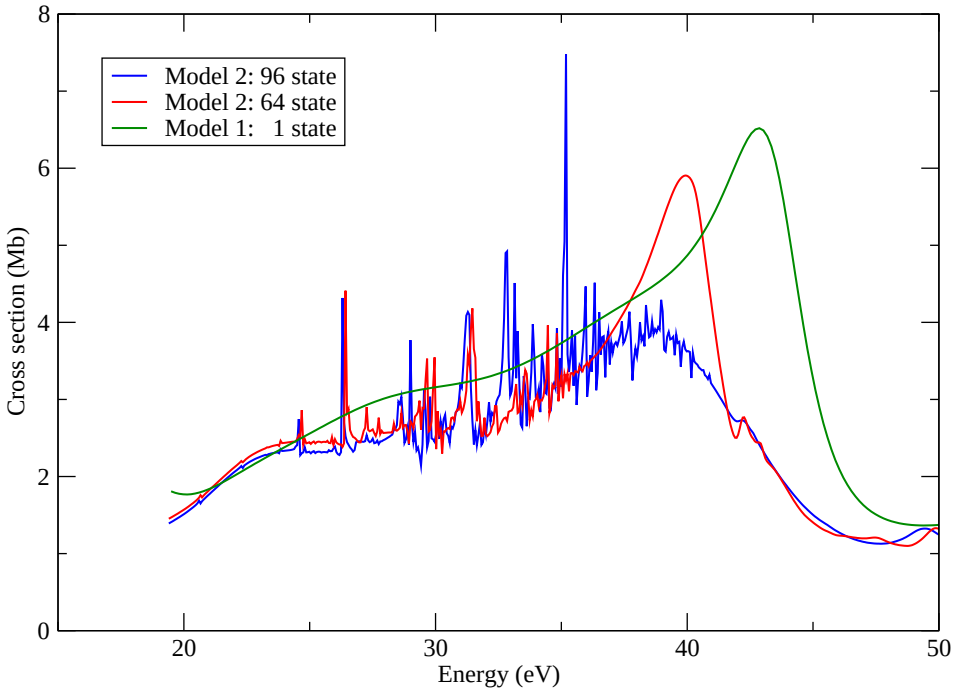

Figure 2: Partial cross sections: Final ion state $C^2\Sigma_g^+$. Comparison of models with different number of ionic states included.

polyatomic molecules.

Appendix

The photoionization dipole in D_{2h}

UKRmol uses real spherical harmonics in the partial wave expansion of the continuum, eq. (7), and to represent the dipole operator when calculating dipoles between molecular orbitals, eq. (3). The lab frame dipole in this basis becomes (dropping the spin related Clebsch-Gordan coefficient for sake of clarity),

$$\boldsymbol{d}_{fi}^{(\mathrm{Re})'}(\boldsymbol{k}'_f) = \sum_{l_f m'_f m_f} i^{-l_f} e^{i\sigma_{l_f}} S_{l_f,m'_f}(\hat{\boldsymbol{k}}'_f) \Delta^l_{m'_f m_f} \boldsymbol{d}^{(\mathrm{Re})}_{f l_f m_f,i}(E) \boldsymbol{\Delta}^{1T}, \quad (32)$$

where $S_{l_f,m'_f}(\hat{\boldsymbol{k}}'_f)$ are the real spherical harmonics and $\Delta^l_{m'_f m_f}(\alpha,\beta,\gamma)$ are the rotation matrices in the basis of real spherical harmonics [55]. For the case of linear molecules, starting in the molecular frame,

$$\boldsymbol{d}_{fi}^{(\mathrm{Re})}(\boldsymbol{k}_f) = \sum_{l_f m_f} i^{-l_f} e^{i\sigma_{l_f}} S_{l_f,m_f}(\hat{\boldsymbol{k}}_f) \boldsymbol{d}^{(\mathrm{Re})}_{f l_f m_f,i}(E), \quad (33)$$

and using the unitary transformation between the real and complex spherical harmonics [55],

$$\boldsymbol{S}_{l_f} = \mathbf{C}^{l_f} \boldsymbol{Y}_{l_f} \quad (34)$$

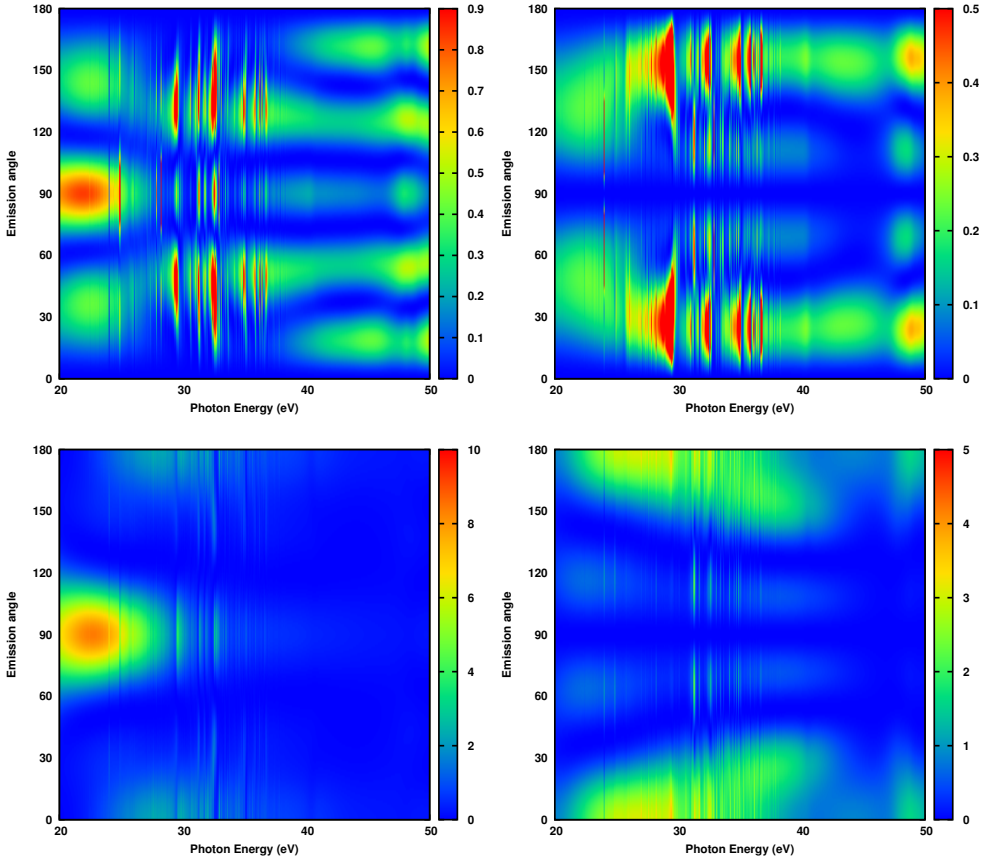

Figure 3: Aligned PAD, the emission angle is defined relative to the lab frame photon polarization (which defines the lab z-axis), the magnitude has units Mb: Top left, $X^2\Pi_g$. Top right, $A^2\Pi_u$. Bottom left, $B^2\Sigma_u^+$. Bottom right, $C^2\Sigma_g^+$

where the spherical harmonics have been written in vector form, we get,

$$\boldsymbol{d}_{fi}(\boldsymbol{k}_f) = \sum_{l_f m_f} i^{-l_f} e^{i\sigma_{l_f}} Y_{l_f,m_f}(\hat{\boldsymbol{k}}_f) \sum_{m'_f} \mathbf{C}^{1\dagger} \boldsymbol{d}^{(\mathrm{Re})}_{f l_f m'_f,i}(E) C^{l_f}_{m'_f m_f}, \quad (35)$$

and identifying,

$$\boldsymbol{d}_{f l_f m_f,i}(E) = \sum_{m'_f} \mathbf{C}^{1\dagger} \boldsymbol{d}^{(\mathrm{Re})}_{f l_f m'_f,i}(E) C^{l_f}_{m'_f m_f}, \quad (36)$$

we recover the molecular frame dipole in the partial wave basis and can transform to the lab frame as before.

Acknowledgements

The authors would like to acknowledge useful discussions with Jonathan Tennyson. We acknowledge the support of Einstein foundation project A-211-55 Attosecond Electron Dynamics.

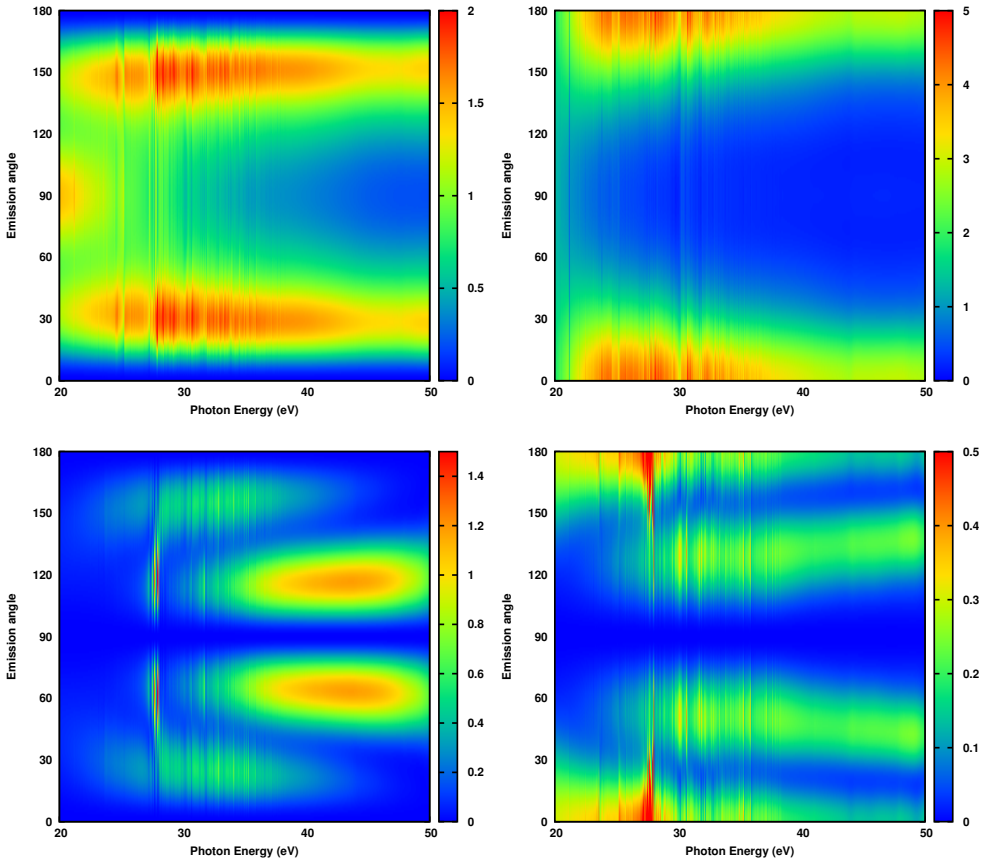

Figure 4: Anti-aligned PAD, the emission angle is defined relative to the lab frame photon polarization (which defines the lab z-axis), the magnitude has units Mb: Top left, $X^2\Pi_g$. Top right, $A^2\Pi_u$. Bottom left, $B^2\Sigma_u^+$. Bottom right, $C^2\Sigma_g^+$

References

[1] S. Baker, J. S. Robinson, C. A. Haworth, H. Teng, R. A. Smith, C. C. Chiril, M. Lein, J. W. G. Tisch, and J. P. Marangos. Probing proton dynamics in molecules on an attosecond time scale. *Science*, 312(5772):424–427, 2006.

[2] Olga Smirnova, Yann Mairesse, Serguei Patchkovskii, Nirit Dudovich, David Villeneuve, Paul Corkum, and Misha Yu Ivanov. High harmonic interferometry of multi-electron dynamics in molecules. *Nature*, 460(7258):972–977, 2009.

[3] S. Haessler, J. Caillat, W. Boutu, C. Giovanetti-Teixeira, T. Ruchon, T. Auguste, Z. Diveki, P. Breger, A. Maquet, B. Carr, R. Taeb, and P. Salires. Attosecond imaging of molecular electronic wavepackets. *Nat. Phys.*, 6(3):200–206, 2010.

[4] M. Schultze, M. Fie, N. Karpowicz, J. Gagnon, M. Korbman, M. Hofstetter, S. Neppl, A. L. Cavalieri, Y. Komninos, Th Mercouris, C. A. Nicolaides, R. Pazourek, S. Nagele, J. Feist, J. Burgdrfer, A. M. Azzeer, R. Ernstorfer, R. Kienberger, U. Kleineberg, E. Goulielmakis, F. Krausz, and V. S. Yakovlev. Delay in Photoemission. *Science*, 328(5986):1658–1662, 2010.

[5] P. M. Paul, E. S. Toma, P. Breger, G. Mullot, F. Aug, Ph Balcou, H. G. Muller, and P. Agostini. Observation of a Train of Attosecond Pulses from High Harmonic Generation. *Science*, 292(5522):1689–1692, 2001.

[6] K. Klnder, J. M. Dahlstrm, M. Gisselbrecht, T. Fordell, M. Swoboda, D. Gunot, P. Johnsson, J. Caillat, J. Mauritsson, A. Maquet, R. Taeb, and A. LHuillier. Probing Single-Photon Ionization on the Attosecond Time Scale. *Phys. Rev. Lett.*, 106(14):143002, 2011.

[7] Michael Spanner, Olga Smirnova, Paul B. Corkum, and Misha Yu Ivanov. Reading diffraction images in strong field ionization of diatomic molecules. *J. Phys. B: At. Mol. Opt. Phys.*, 37(12):L243, 2004.

[8] M. Meckel, D. Comtois, D. Zeidler, A. Staudte, D. Pavii, H. C. Bandulet, H. Ppin, J. C. Kieffer, R. Drner, D. M. Villeneuve, and P. B. Corkum. Laser-Induced Electron Tunneling and Diffraction. *Science*, 320(5882):1478–1482, 2008.

[9] Cosmin I. Blaga, Junliang Xu, Anthony D. DiChiara, Emily Sistrunk, Kaikai Zhang, Pierre Agostini, Terry A. Miller, Louis F. DiMauro, and C. D. Lin. Imaging ultrafast molecular dynamics with laser-induced electron diffraction. *Nature*, 483(7388):194–197, 2012.

[10] Misha Yu. Ivanov, Thomas Brabec, and Neal Burnett. Coulomb corrections and polarization effects in high-intensity high-harmonic emission. *Phys. Rev. A*, 54(1):742–745, 1996.

[11] Cheng Jin, Anh-Thu Le, and C. D. Lin. Retrieval of target photorecombination cross sections from high-order harmonics generated in a macroscopic medium. *Phys. Rev. A*, 79(5):053413, 2009.

[12] Misha Ivanov and Olga Smirnova. How Accurate Is the Attosecond Streak Camera? *Phys. Rev. Lett.*, 107(21):213605, 2011.

[13] Anh-Thu Le, R. R. Lucchese, S. Tonzani, T. Morishita, and C. D. Lin. Quantitative rescattering theory for high-order harmonic generation from molecules. *Phys. Rev. A*, 80(1):013401, 2009.

[14] J. M. Carr, P. G. Galiatsatos, J. D. Gorfinkiel, A. G. Harvey, M. A. Lysaght, D. Madden, Z. Man, M. Plummer, J. Tennyson, and H. N. Varambhia. Ukrmol: a low-energy electron- and positron-molecule scattering suite. *Eur. Phys. J. D*, 66(3):1–11, 2012.

[15] Jonathan Tennyson and N. Chandra. PEAD - for the calculation of photoelectron angular distributions of linear molecules. *Comp. Phys. Comm.*, 46(1):99–105, 1987.

[16] J. Tennyson. Fully vibrationally resolved photoionisation of H_2 and D_2. *J. Phys. B: At. Mol. Phys.*, 20(12):L375, 1987.

[17] J. Colgan, D. H. Glass, K. Higgins, and P. G. Burke. R-matrix Floquet theory of molecular multiphoton processes: II. Multiphoton ionization of H_2. *J. Phys. B: At. Mol. Opt. Phys.*, 34(11):2089, 2001.

[18] Motomichi Tashiro. Application of the R-matrix method to photoionization of molecules. *J. Chem. Phys.*, 132(13):134306, 2010.

[19] Stefano Tonzani. FERM3D: A finite element R-matrix electron molecule scattering code. *Comp. Phys. Comm.*, 176(2):146–156, 2007.

[20] E. P. Wigner and L. Eisenbud. Higher Angular Momenta and Long Range Interaction in Resonance Reactions. *Phys. Rev.*, 72(1):29–41, 1947.

[21] Jonathan Tennyson. Electron-molecule collision calculations using the R-matrix method. *Phys. Rep.*, 491(2):29–76, 2010.

[22] P. G. Burke. *R-Matrix Theory of Atomic Collisions: Application to Atomic, Molecular and Optical Processes*. Springer, 2011.

[23] H. A. Bethe and E. E. Salpeter. *Quantum Mechanics of One- and Two-Electron Systems*, pages 88–436. Number 7 / 35 in Encyclopedia of Physics / Handbuch der Physik. Springer Berlin Heidelberg, 1957.

[24] D. M Brink and G. R Satchler. *Angular momentum*. Clarendon Press ; Oxford University Press, 1993.

[25] P. G. Burke. *Electron and Photon Collisions with Molecules*, pages 69–122. Springer US, 1982.

[26] Alexandre Faure, Jimena D Gorfinkiel, Lesley A Morgan, and Jonathan Tennyson. GTOBAS: fitting continuum functions with Gaussian-type orbitals. *Comp. Phys. Comm.*, 144(2):224–241, 2002.

[27] Jonathan Tennyson. A new algorithm for Hamiltonian matrix construction in electron-molecule collision calculations. *J. Phys. B: At. Mol. Opt. Phys.*, 29(9):1817, 1996.

[28] K. L. Baluja, P. G. Burke, and L. A. Morgan. R-matrix propagation program for solving coupled second-order differential equations. *Comp. Phys. Comm.*, 27(3):299–307, 1982.

[29] B. K. Sarpal, S. E. Branchett, J. Tennyson, and L. A. Morgan. Bound states using the R-matrix method: Rydberg states of HeH. *J. Phys. B: At. Mol. Opt. Phys.*, 24(17):3685, 1991.

[30] Alex G. Harvey, Danilo S. Brambila, Felipe Morales, and Olga Smirnova. CDENPROP: Transition matrix elements involving continuum states. *arXiv:1401.0229 [physics]*, 2013.

[31] Alex G. Harvey and Jonathan Tennyson. Electron re-scattering from H_2 and CO_2 using R-matrix techniques. *J. Mod. Opt.*, 54(7):1099–1106, 2007.

[32] A. G. Harvey and J. Tennyson. Electron re-scattering from aligned linear molecules using the R-matrix method. *J. Phys. B: At. Mol. Opt. Phys.*, 42(9):095101, 2009.

[33] Alex G. Harvey and Jonathan Tennyson. *The R-matrix Calculations of Orientation and Coulomb Phase Effects in Electron-Molecule (Re-)Collisions*, pages 55–70. CRM Series in

Mathematical Physics. Springer New York, 2011.

[34] Thom H. Dunning Jr. Gaussian basis sets for use in correlated molecular calculations. I. the atoms boron through neon and hydrogen. *J. Chem. Phys.*, 90(2):1007–1023, 1989.

[35] Peter J. Knowles and H.-J. Werner. An Efficient Second Order MCSCF Method for Long Configuration Expansions. *Chem. Phys. Lett.*, 115:259267, 1985.

[36] Hans-Joachim Werner and Peter J. Knowles. A second order multiconfiguration SCF procedure with optimum convergence. *J. Chem. Phys.*, 82(11):5053–5063, 1985.

[37] H.-J. Werner, P. J. Knowles, G. Knizia, F. R. Manby, M. Schtz, P. Celani, T. Korona, R. Lindh, A. Mitrushenkov, G. Rauhut, K. R. Shamasundar, T. B. Adler, R. D. Amos, A. Bernhardsson, A. Berning, D. L. Cooper, M. J. O. Deegan, A. J. Dobbyn, F. Eckert, E. Goll, C. Hampel, A. Hesselmann, G. Hetzer, T. Hrenar, G. Jansen, C. Kppl, Y. Liu, A. W. Lloyd, R. A. Mata, A. J. May, S. J. McNicholas, W. Meyer, M. E. Mura, A. Nicklass, D. P. O'Neill, P. Palmieri, D. Peng, K. Pflger, R. Pitzer, M. Reiher, T. Shiozaki, H. Stoll, A. J. Stone, R. Tarroni, T. Thorsteinsson, and M. Wang. *MOLPRO, version 2012.1, a package of ab initio programs*. 2012.

[38] F. Kelkensberg, A. Rouze, W. Siu, G. Gademann, P. Johnsson, M. Lucchini, R. R. Lucchese, and M. J. J. Vrakking. XUV ionization of aligned molecules. *Phys. Rev. A*, 84(5):051404, 2011.

[39] Robert R. Lucchese. Effects of interchannel coupling on the photoionization cross sections of carbon dioxide. *J. Chem. Phys.*, 92(7):4203–4211, 1990.

[40] Robert R. Lucchese and Vincent McKoy. Vibrational effects in the photoionization shape resonance leading to the $C^2\Sigma_g^+$ state of CO_2^+. *Phys. Rev. A*, 26(4):1992–1996, 1982.

[41] Robert R. Lucchese and Vincent McKoy. Studies of differential and total photoionization cross sections of carbon dioxide. *Phys. Rev. A*, 26(3):1406–1418, 1982.

[42] J. D. Gorfinkiel and J. Tennyson. Electron impact ionization of small molecules at intermediate energies: the molecular R-matrix with pseudostates method. *J. Phys. B: At. Mol. Opt. Phys.*, 38(11):1607, 2005.

[43] James A. R. Samson and J. L. Gardner. Fluorescence excitation and photoelectron spectra of CO_2 induced by vacuum ultraviolet radiation between 185 and 716 Angstroms. *J. Geophys. Res.*, 78(19):36633667, 1973.

[44] T. Gustafsson, E. W. Plummer, D. E. Eastman, and W. Gudat. Partial photoionization cross sections of CO_2 between 20 and 40 eV studied with synchrotron radiation. *Phys. Rev. A*, 17(1):175–181, 1978.

[45] M. R. F. Siggel, J. B. West, M. A. Hayes, A. C. Parr, J. L. Dehmer, and I. Iga. Shape-resonance-enhanced continuum-continuum coupling in photoionization of CO_2. *J. Chem. Phys.*, 99(3):1556–1563, 1993.

[46] C. E. Brion and K. H. Tan. Partial oscillator strengths for the photoionization of N_2O and CO_2 (2060 eV). *Chem. Phys.*, 34(2):141–151, 1978.

[47] P. Roy, I. Nenner, M. Y. Adam, J. Delwiche, M. J. Hubin Franskin, P. Lablanquie, and D. Roy. On the photoionization shape resonance associated to the $C^2\Sigma_2^+$ state of CO_2^+. *Chem. Phys. Lett.*, 109(6):607–614, 1984.

[48] Bretislav Friedrich and Dudley Herschbach. Alignment and Trapping of Molecules in Intense Laser Fields. *Phys. Rev. Lett.*, 74(23):4623–4626, 1995.

[49] G. Ravindra Kumar, P. Gross, C. P. Safvan, F. A. Rajgara, and D. Mathur. Molecular pendular states in intense laser fields. *Phys. Rev. A*, 53(5):3098–3102, 1996.

[50] Tamar Seideman. Revival Structure of Aligned Rotational Wave Packets. *Phys. Rev. Lett.*, 83(24):4971–4974, 1999.

[51] Henrik Stapelfeldt and Tamar Seideman. Colloquium: Aligning molecules with strong laser pulses. *Rev. Mod. Phys.*, 75(2):543–557, 2003.

[52] Guiping Zeng, Fengjiao Zhong, Chengyin Wu, Hongbing Jiang, and Qihuang Gong. Field-free molecular alignment and its application. *Laser Phys.*, 19(8):1691–1696, 2009.

[53] Katharine L. Reid. Photoelectron Angular Distributions. *Annu. Rev. Phys. Chem.*, 54(1):397–424, 2003.

[54] A. Rouzee, A. G. Harvey, F. Kelkensberg, D. S. Brambila, Wing Kiu Siu, G. Gademann, O. Smirnova, and M. J. J. Vrakking. Submitted for publication.

[55] Miguel A. Blanco, M. Flrez, and M. Bermejo. Evaluation of the rotation matrices in the basis of real spherical harmonics. *J. Mol. Struct. (Theochem)*, 419(1):19–27, 1997.